Raman investigation of stable and metastable states of 4-octyl-4′-cyanobiphenyl confined in porous silica matrices

C. Fehr, P. Dieudonné, J. L. Sauvajol, and E. Anglaret
Groupe de Dynamique des Phases Condensées, UMR CNRS 5581, Université Montpellier II, 34095 Montpellier Cedex 5, France
(Received 19 November 2002; published 23 June 2003)

We study the polymorphism of solid phases of 4-octyl-4′-cyanobiphenyl (8CB) by Raman spectroscopy. For bulk 8CB, the Raman spectrum of the CN stretch is featured by a single peak, which shifts abruptly at the smectic-*A*–crystal transition. In confinement, the CN peak splits both at high and low temperatures. In the isotropic and liquid crystal phases, the signature of the liquid crystal bulk (LC) coexists with another peak that is assigned to LC molecules interacting with the matrice interface. We find correlations between the volumic fractions of interfacial liquid and the texture of the matrices. At low temperatures, we assign the splitting of the CN peak to the coexistence of different metastable solid phases. For strong confinements, the temperature dependence of the CN stretching frequency extends to that of the liquid, which suggests the existence of frozen-in smecticlike solid phases. We discuss the structure of these metastable solid phases in the light of neutron diffraction measurements. We also report on the peculiar analogy between the effect of quenched disorder due to the porous matrices and the effect of thermal quenching.

DOI: 10.1103/PhysRevE.67.061706 PACS number(s): 64.70.Md, 61.30.−v, 78.30.Jw

I. INTRODUCTION

The effect of confinement on the physical properties of fluids is a subject of increasing interest [1,2]. Thermotropic liquid crystals (LC) are model materials for testing such effects, since they offer a wide choice of structures and phase transitions in a relatively narrow temperature range. Intensive work was carried out to study the effect of confinement or quenched disorder on the phase transitions [3,4] and the structure [3,5–8] of mesomorph phases. So far, structural and dynamical studies of LC essentially focused on the mesomorph phases because of their original physical and electro-optical properties and their wide range of applications. Much less studies focused on the structure of crystalline phases. However, LC-forming compounds are known to present solid crystalline polymorphism (SCP). The SCP was even proposed to be a necessary condition for a compound to present some mesomorph phases [9,10]. Moreover, the structure and molecular organization of mesophases is likely strongly related to those of the metastable solid phases. Therefore, deep studies of the polymorphism of solid phases are required to better describe the properties of liquid crystal phases.

The SCP in bulk LC materials was studied by coupled Differential Scanning Calorimetry and x-ray scattering on monocrystals or powders [11–15] and by Raman scattering [9–11,16]. Extensive studies of 4-methoxybenzylidene-4′-*n*-butylaniline and 4-ethoxybenzylidene-4′-*n*-butylaniline (EBBA) were achieved [11–14]. The phase diagrams of these compounds include a glassy nematic state obtained after thermal quenching at low temperatures (only for EBBA), and three or four metastable SCP obtained upon heating after thermal quenching, including ''smecticlike'' monolayer or bilayer solid phases. The phase diagram of metastable states for the 4-*n*-alkyl-4′-cyanobiphenyl (*n*CB) family is not yet well understood. These compounds are, however, of primary interest because mixtures, and in a smaller extent pure molecules, of *n*CB present nematic- and smectic-*A* phases on rather large domains of temperatures around room temperature. Therefore, *n*CB compounds are probably the most widely used LC both in academic studies and in industrial applications. Raman spectroscopy was used by several groups to study SCP in these compounds. Ogorodnik proposed that three or four solid crystalline phases can be formed by modifying the cooling rate of *n*CB ($n=4–8$), each phase being characterized either by a single peak or by a doublet in the CN range [10]. Bulkin *et al.* proposed that the structure of the metastable phases corresponds to a quenched nematic phase [9]. Jaffrain *et al.* studied in detail the Raman response of the alkyl chain and concluded that the mobility of the chains was much larger for the metastable phase due to a smaller compacity of the network [16]. Perrot *et al.* reported a Raman study of stable and metastable crystalline phases of *n*CB [17–19]. For $n=8–12$, a metastable phase is formed after thermal quenching from the isotropic phase. In variance with Bulkin *et al.*, these authors propose that the structure of the metastable phases corresponds to a frozen-in, smecticlike phase. By contrast, for $n=1$ and $n=6$, no metastable phase could be observed in their study, in variance with the results obtained by Ogorodnik [10]. More recently, Hori *et al.* studied polymorphism in 4-*n*-alkyloxy-4′-cyanobiphenyls (with $n=6–12$) and directly observed the growth of three to four different monocrystalline phases of different shapes from aceton solutions.

In this paper, we study the influence of confinement on SCP of 8CB. The LC were confined in a series of disordered silica porous matrices of different pore-size distributions and surface textures. We find SCP and study the vibrational dynamics of the metastable solid phases at low temperatures by Raman scattering both after slow cooling and after thermal quenching. We discuss the effect of anchoring on silica surfaces on the formation of metastable phases and underline analogies between the effects of quenched disorder and thermal quenching. We discuss the structure of the metastable

TABLE I. Compared textures of the porous matrices used for confined 8CB. d is the mean pore size, ρ is the apparent density, and ϕ_{pore} is the porosity (volume fraction of pores), $S_{sp,BJH}$ is the specific area estimated from N_2 adsorption experiments (see text), $S_{sp,SAXS}$ is the specific area estimated from small angle x-ray scattering experiments, and S_V is the surface of silica per unit of porous volume.

Sample	d (nm)	ρ (g cm^{-3})	ϕ_{pore}	$S_{sp,BET}$ (m^2 g^{-1})	$S_{sp,SAXS}$ (m^2 g^{-1})	S_V (m^2 cm^{-3})
XA20	20 ± 1.5	0.44	80	267 ± 11	245 ± 15	140 ± 14
XA17	17 ± 1	0.57	74	273 ± 11	269 ± 16	209 ± 15
XA10	10 ± 1	1.08	51	151 ± 6	143 ± 9	315 ± 26

phases in the light of neutron diffraction experiments. Finally, we correlate Raman and diffraction results, and attempt to provide a clear picture of SCP in 8CB.

II. EXPERIMENT

A. Preparation of the samples

4-octyl-4′-cyanobiphenyl was purchased from Merck and used without further purification. The sequence of phases for bulk 8CB is crystal (K)–smectic A (A)–nematic (N)–isotropic (I), and the phase transitions upon slow heating from the crystalline phase occur at $T_{KA}=21.5\,^{\circ}$C (first order), $T_{AN}=33.7\,^{\circ}$C (second order), and $T_{NI}=40.5\,^{\circ}$C (weakly first order). Silica porous matrices were prepared through a two-step drying procedure followed by a partial densification by heat treatment [20]. The samples prepared by this original process are called xeroaerogels (XA). This allowed us to prepare a series of samples, which present the same structure at a microscopic scale, i.e., dense silica essentially covered by OH groups, and different textures at mesoscopic scales. Their textures were carefully characterized by N_2 adsorption-desorption isotherms and small angle x-ray scattering (SAXS) [20]. The distribution of pore size was determined from a Barret-Joyner-Halenda analysis of the isotherms assuming cylindrical pores. The specific area was estimated from a Brunauer-Emmett-Teller analysis and from the SAXS results. Results are presented in Table I. Hereafter, we label the samples XAn where XA is for xeroaerogels and n is the mean size of the pores in nanometers. The sol-gel samples were filled under a He atmosphere in order to favor gas diffusion in the LC around 330 K, i.e., with the LC in the isotropic phase.

B. Raman scattering experiments

Raman spectra were recorded with a T64000 Jobin-Yvon spectrometer using the 647.1-nm radiation of an Ar/Kr ion laser in a 90° scattering geometry. Bulk sample was studied in a Hellma cell of thickness 1 mm. For each set of measurement, the sample was first heated at 330 K, above the temperature of the NI transition in the bulk. A direct optical check confirmed that the LC were in the isotropic phase for all samples. The sample was then ''quenched'' down to 100 K by inserting the sample in a cryostat already stabilized at this temperature. The typical time for stabilizing the temperature of the sample at 100 K was about 45 min. At high temperatures, we also performed measurements of the Raman depolarization ratio ρ, i.e., the ratio of Raman intensity between crossed polarizers (vertical/horizontal configuration) and between parallel polarizers (vertical/vertical configuration). We will show that the temperature dependence of ρ is a relevant probe of the NI transition.

C. Neutron diffraction experiments

Neutron diffraction (ND) experiments were performed on the D16 diffractometer at the Institut Laue Langevin (Grenoble, France) and on the G6-1 diffractometer at the Laboratoire Léon Brillouin (Saclay, France) using incident neutrons of wavelengths 4.54 Å and 4.78 Å, respectively. The samples were placed in aluminum foils in order to limit the scattering from the container. The data were corrected from scattering contribution from the aluminum foil. In order to remove the strong scattering contribution at small angles from the porous matrices and strong incoherent signal from the hydrogens, we susbstracted to each pattern the pattern measured in the isotropic phase. A detailed presentation of the experimental results on two different series of samples will be published elsewhere [21]. In this paper, we present only a selection of results for the series of xeroaerogels in the smectic-A phase, and at low temperatures for both slow cooling and thermal quenching from the isotropic phase.

III. RESULTS AND INTERPRETATION

A. Raman results for bulk 8CB

Figure 1 displays typical Raman spectra of bulk 8CB at 320 K (isotropic phase). The range of frequencies below 200 cm^{-1} corresponds essentially to intermolecular and deformation modes (not shown), while the range of frequencies between 200 and 3200 cm^{-1} corresponds essentially to intramolecular vibrations and, more specifically, to stretching modes between 1200 and 3200 cm^{-1}. A complete assignment of the Raman peaks in this latter frequency range can be found in the literature [18,22]. As expected, only a few differences are observed between the spectra of intramolecular modes measured at different temperatures (not shown, see Ref. [18] and also Ref. [23] for an infrared study). The changes in the frequency range of the CH stretch have been studied in detail in Refs. [16,23]. These provide information on the conformations of the alkyl chains. Three other peaks are observed to shift at the smectic-A–crystal transitions: the C—C, C═C, and CN stretches and the largest shift is observed for the CN mode [23]. Note that the A_1 CN stretching

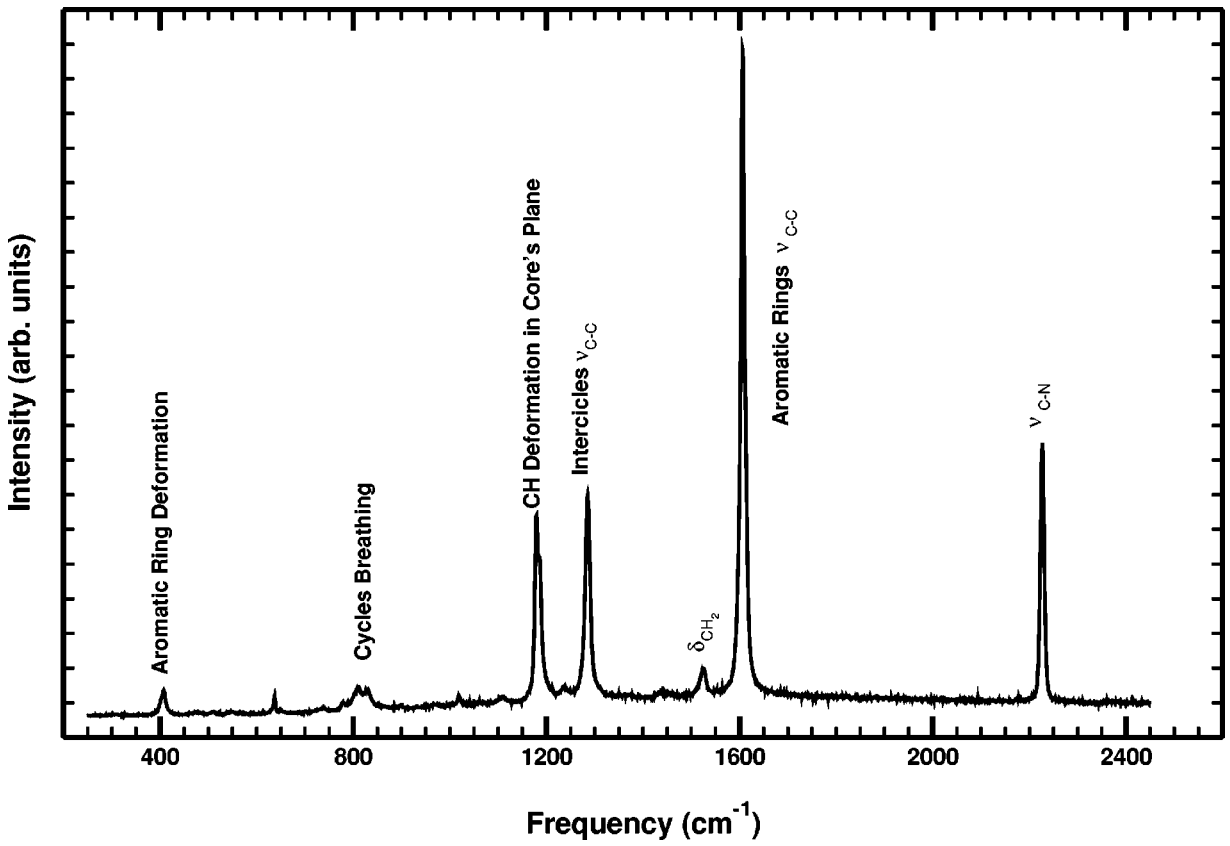

FIG. 1. Raman spectra of the bulk 8CB at 320 K (isotropic liquid I).

mode has been used as a useful tool to study the orientational order in cyanobiphenyl compounds from the polarized Raman spectroscopy, since its motion is parallel to the main axis of the molecule [24,25]. We checked that the frequency of the CN stretching mode was the most sensitive probe to scan the *KA* transition. This is emphasized in Figs. 2 and 3 that display a set of CN spectra for bulk 8CB. The CN stretching frequency relates to the local environment of the molecules. This shift is due to different molecular packing in the crystalline phase with respect to the liquid (crystal) phases and to the coupling of CN oscillators in the periodic arrangement of the crystalline phase. By contrast, the signatures observed in all liquid (crystal) phases are similar and correspond to the Raman signatures of the isolated molecule. This indicates that intermolecular interactions are too weak in the liquid phases to induce significant changes in the Raman spectra with respect to the spectra of the isolated molecule. Several studies addressed the structure of the smectic-

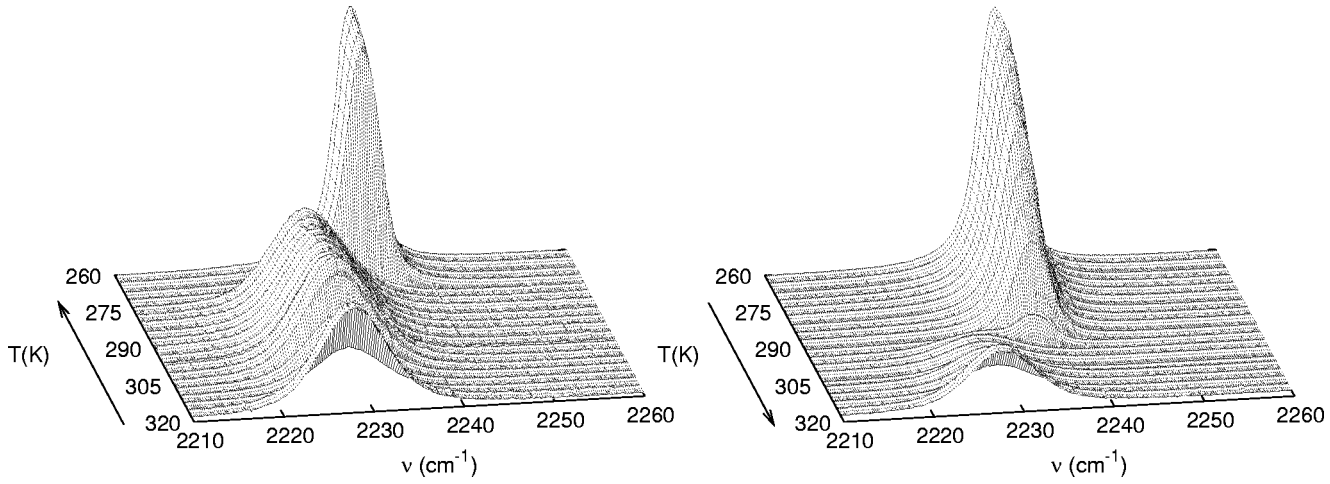

FIG. 2. Raman spectra of the CN stretch for bulk 8CB at various temperatures. Left: slow cooling from the isotropic phase. Right: slow heating after a ''soft'' thermal quench at 100 K.

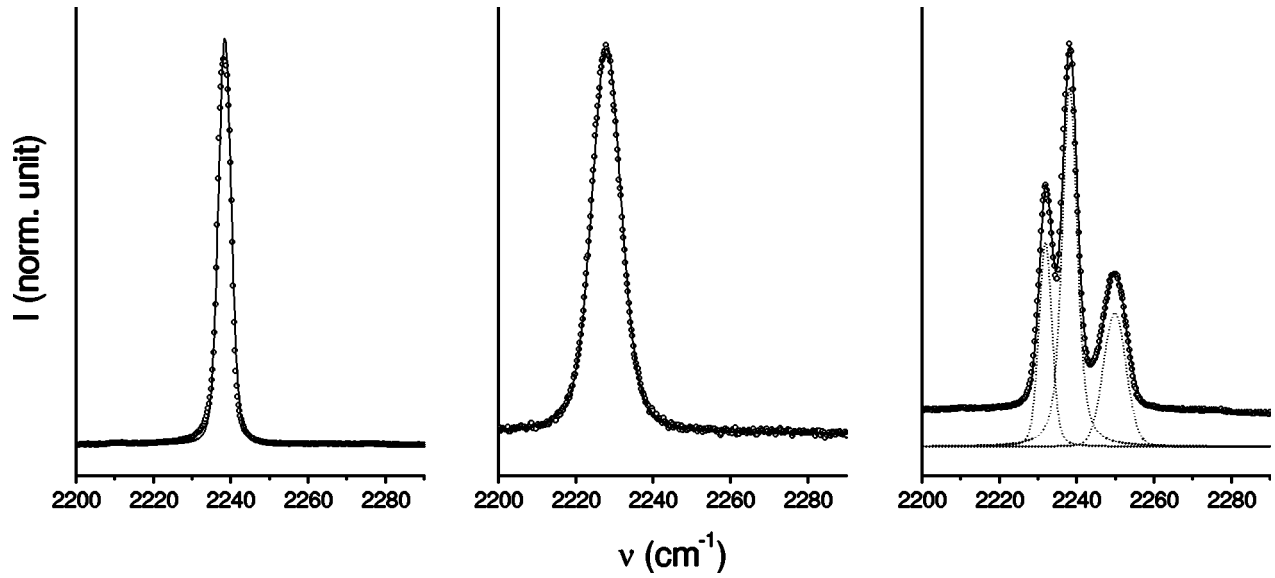

FIG. 3. Typical fits of the Raman spectra for the bulk 8CB. Left: at 135 K after slow cooling from the isotropic phase. Center: at 320 K. Right: at 135 K after a ''hard'' thermal quench from the isotropic phase (see text).

A phase for cyanobiphenyl compounds [22,26,27]. The picture which is generally accepted is the formation of couples of molecules in an antiparallel packing with an overlap of the biphenyl groups. These couples align to form smectic layers in the smectic-*A* phase. Small smectic clusters already exist in the nematic phase, and couples of molecules likely already exist even above the *NI* transition.

The results obtained upon quenching were not reproducible. This is due to the cooling speed during thermal quench which is not well controlled in our experiment and may be insufficiently large to form the metastable phase. In some cases (hereafter referred as ''soft'' quenchs), the results were very close to what is obtained by slow cooling (Fig. 2, right). In other cases (hereafter referred to as ''hard'' quenchs), one observes a splitting of the CN peak after thermal quenching (Fig. 3, right). We assign the splitting of the nondegenerate CN mode to the coupling of different CN oscillators in one or several different crystalline lattices. De Zen *et al.* already reported the observation of such a splitting and assigned it to the formation of a solid crystalline metastable phase. They also underlined that it was rather difficult to obtain this metastable state through thermal quenching [18]. The three main components of the spectrum are located around 2232, 2238, and 2249 cm^{-1}, in good agreement with the results of Ref. [18]. However, the respective intensities of the peaks are different, which suggest a coexistence of different solid phases, each one featured by one or two peaks in the Raman spectrum.

The spectra in the frequency range of the CN peak were fitted by a series of Voigt functions. Typical fits at high (isotropic phase, similar fits are achieved in the nematic- and smectic-*A* phases) and low (solid phases) temperatures are presented in Fig. 3. When the stable crystalline phase *K* is formed at low temperatures, good fits can be achieved for all spectra with a single line (Fig. 3, left). Note that the fit with a Voigt function is used to probe the temperature dependence of the CN frequency, but does not provide much information on the dynamics of the molecules. The spectra in the liquid (crystal) phases can also be fitted with a single Voigt line (Fig. 3, center). As expected, the width of the peak is significantly larger in the liquid with respect to the solid. By contrast, at least three Voigt functions are required to achieve a good fit of the spectrum measured at low temperatures after hard thermal quenching (Fig. 3, right). The shape and frequency of the second component are close to that measured after slow cooling, suggesting the presence of the *K* phase. However, its width is slightly larger, which can be assigned to disorder and/or to a smaller crystalline coherence length. The two other components are assigned to one or several metastable solid phase(s). The width of the highest frequency component is particularly large, suggesting a strong disorder and/or ill-crystallized structures.

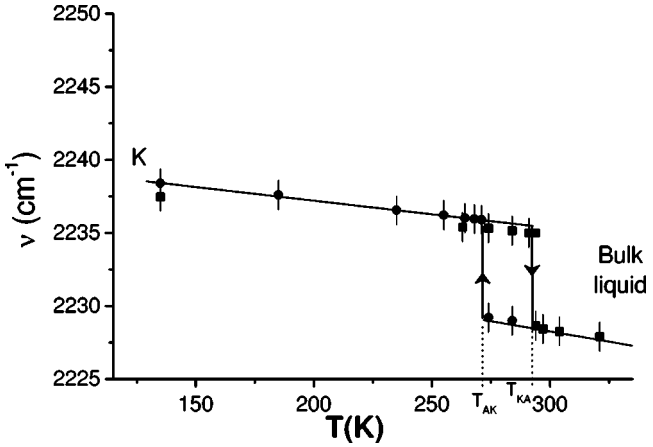

FIG. 4. Temperature dependence of the CN stretching frequency for the bulk 8CB when the stable (*K*) crystal is formed after thermal quench. Circles correspond to slow cooling from the isotropic phase. Squares correspond to slow heating after thermal quench at 100 K. Solid lines are guides for the eyes. Vertical dotted lines indicate the temperatures of the smectic-*A*–crystal (cooling) and crystal–smectic-*A* (heating) transition.

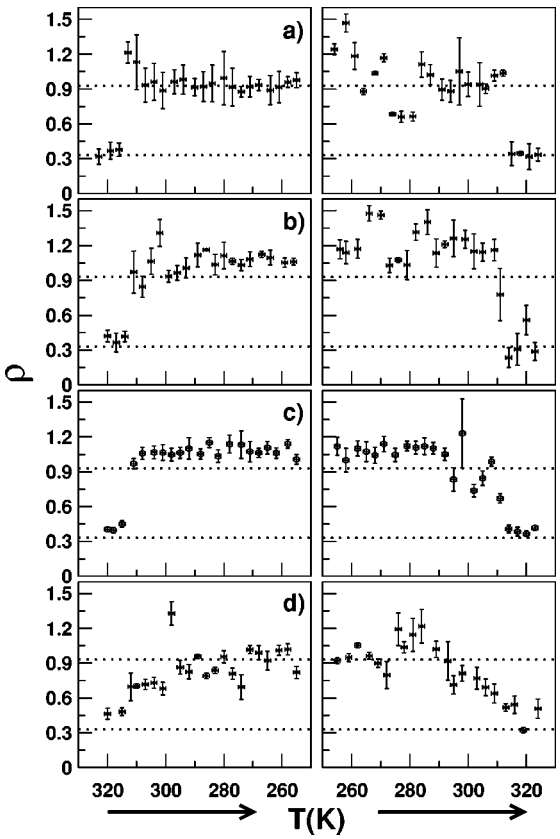

FIG. 5. Raman depolarization ratio for the CN stretch of the bulk 8CB (a) and 8CB confined in sample XA20 (b), in sample XA17 (c) and in sample XA10 (d). Left: slow cooling. Right: slow heating after a thermal quench. The dotted lines indicate the value of the depolarization ratio in the bulk at the isotropic and nematic plateaus.

Figure 4 displays the temperature dependence of the CN frequency for slow cooling and slow heating after a soft thermal quench. The abrupt shift of the frequency is typical of the first-order smectic-A–crystal transition. As expected, this transition is also characterized by a hysteresis but on both sides of the transition, the results obtained upon heating after quench and upon slow cooling are found to be very close to each other. It states, in particular, that the properties of the liquid phases are not sensitive to the thermal history of the sample. No signature of the *IN* or *NA* transition is observed from the temperature-dependence of the CN frequency. Indeed, the frequency of the CN peak presents a slow and continuous temperature dependence from the isotropic phase to the smectic-A–crystal transition.

By contrast, the *NI* transition can be probed through the temperature dependence of the Raman depolarization ratio ρ. The results are presented in Fig. 5. The depolarization ratio is close to 0.33 in the isotropic phase, as already reported elsewhere [18]. It increases abruptly at the isotropic-nematic transition up to a value close to 0.93, which is a forbidden value for isotropic liquids [28]. The depolarization ratio is sensitive to the anisotropy of the Raman polarizability tensor. The form of the Raman tensor depends on point symmetry, which is different for the molecule in the isotropic phase and in the nematic phase. By contrast, no signature of the *NA* transition is observed, which can be understood since both phases present cylindrical symmetry. The *NI* transition is rather sharp in the bulk. A weak hysteresis is observed between cooling and heating, as expected for this (weakly) first-order transition. No other dependence on thermal history can be observed.

B. Effect of confinement on the Raman signatures

Figures 6 and 7 present sets of Raman spectra at various temperatures for 8CB confined in xeroaerogels. Drastic changes are observed with respect to the bulk. For all matrices at all temperatures, the CN peak splits into two or three components. In the largest pores (sample XA20), the effect is rather weak [Figs. 6(a) and 7(a)]. Upon slow cooling, the spectra are dominated by the signature of the bulk both in the liquid and in the solid phases. However, one observes a small additional component, upshifted with respect to the bulk in the liquid phases and down-shifted with respect to the bulk in the solid phase. After a thermal quench, the main signature is the same as for slow cooling, but the intensity of the left-side satellite increases and a third component is observed on the right side of the main peak at low temperatures [Figs. 6(a) and 7(a), right]. The spectrum is actually very close to that measured in the bulk after a hard thermal quench (Fig. 3, right), except that the width of the peaks is significantly larger. This broadening is assigned to a shorter spatial extension of the CN modes coupling, as expected for smaller crystal sizes in confined geometry, and/or to incomplete order that prevents the $k=0$ selection rule conditions to be fulfilled for the optical modes. The Raman signatures observed for 8CB confined in sample XA17 are qualitatively the same as that for sample XA20, but the intensities of the satellites increase at the expense of the peak characteristic of the bulk [Figs. 6(b) and 7(b)]. Especially, after a thermal quench, the intensity of the low-frequency component becomes the most important in the spectrum at low temperatures. Note that its width is narrower than that for sample XA20 after a thermal quench, suggesting a larger crystal size for the metastable phase in sample XA17. This seems surprising since confinement is stronger in sample XA17 than that in sample XA20. In our opinion, it must be assigned to the growth of metastable domains to the expense of stable crystal domains, which is also supported by the increase of the peak intensity. Finally, for the strongest confinement (sample XA10), the spectra are completely dominated by the lowest frequency peak, especially after a thermal quench [Figs. 6(c) and 7(c)]. The width of this peak clearly increases with respect to the other samples, which indicates much more severe confinement.

For confined 8CB, at any temperature, the CN spectra cannot be fitted anymore with a single Voigt function. Two or three components are required to achieve good fits of the data (Fig. 7). The following five general features of the effect of confinement on the Raman spectrum of 8CB can be pointed out.

(i) The location of the peaks seems to be almost sample-independent, only the respective intensities change from one

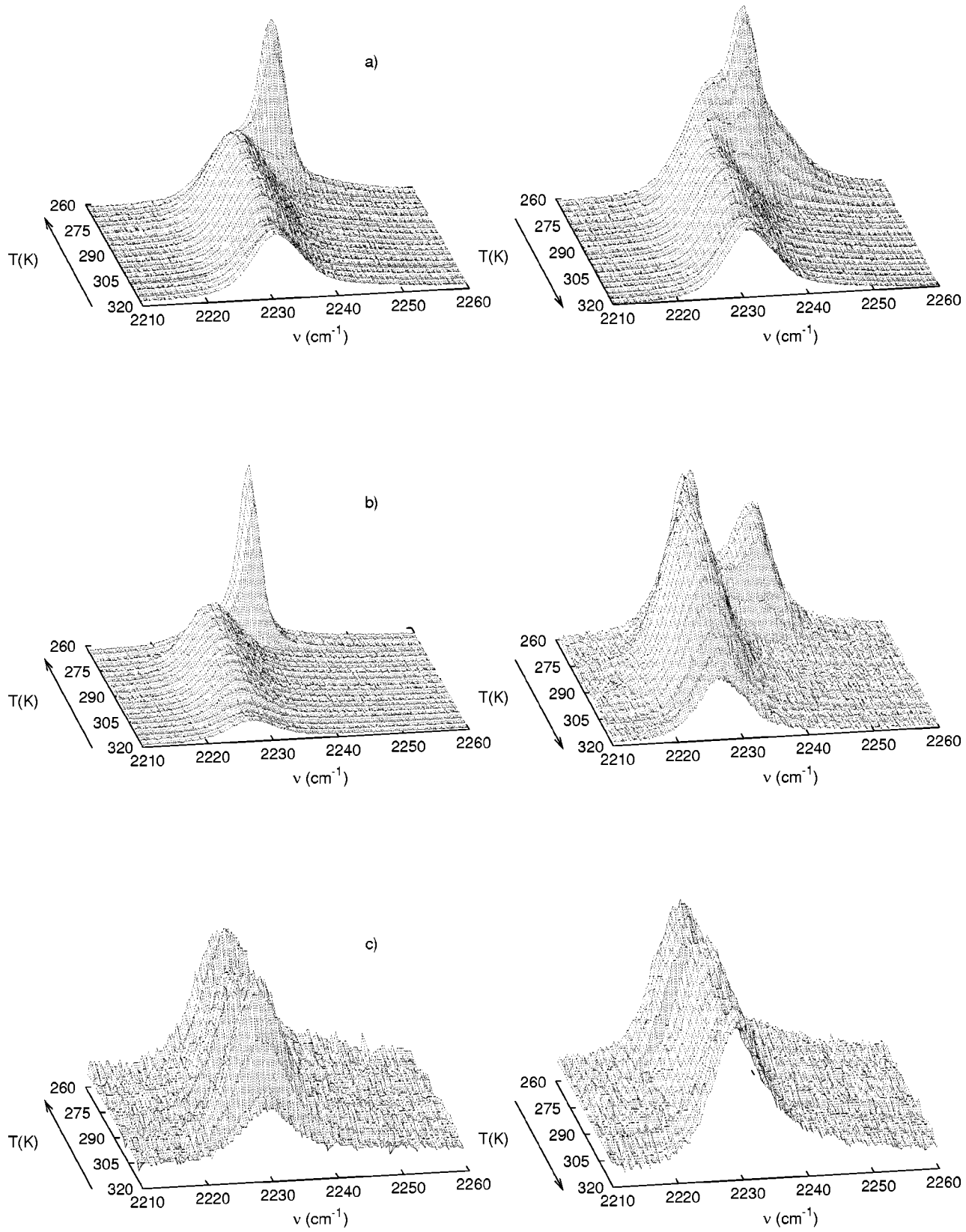

FIG. 6. Raman spectra of the CN stretch at various temperatures for confined 8CB in samples (a) XA20, (b) XA17, (c) XA10. Left: slow cooling from the isotropic phase. Right: slow heating after a thermal quench at 100 K.

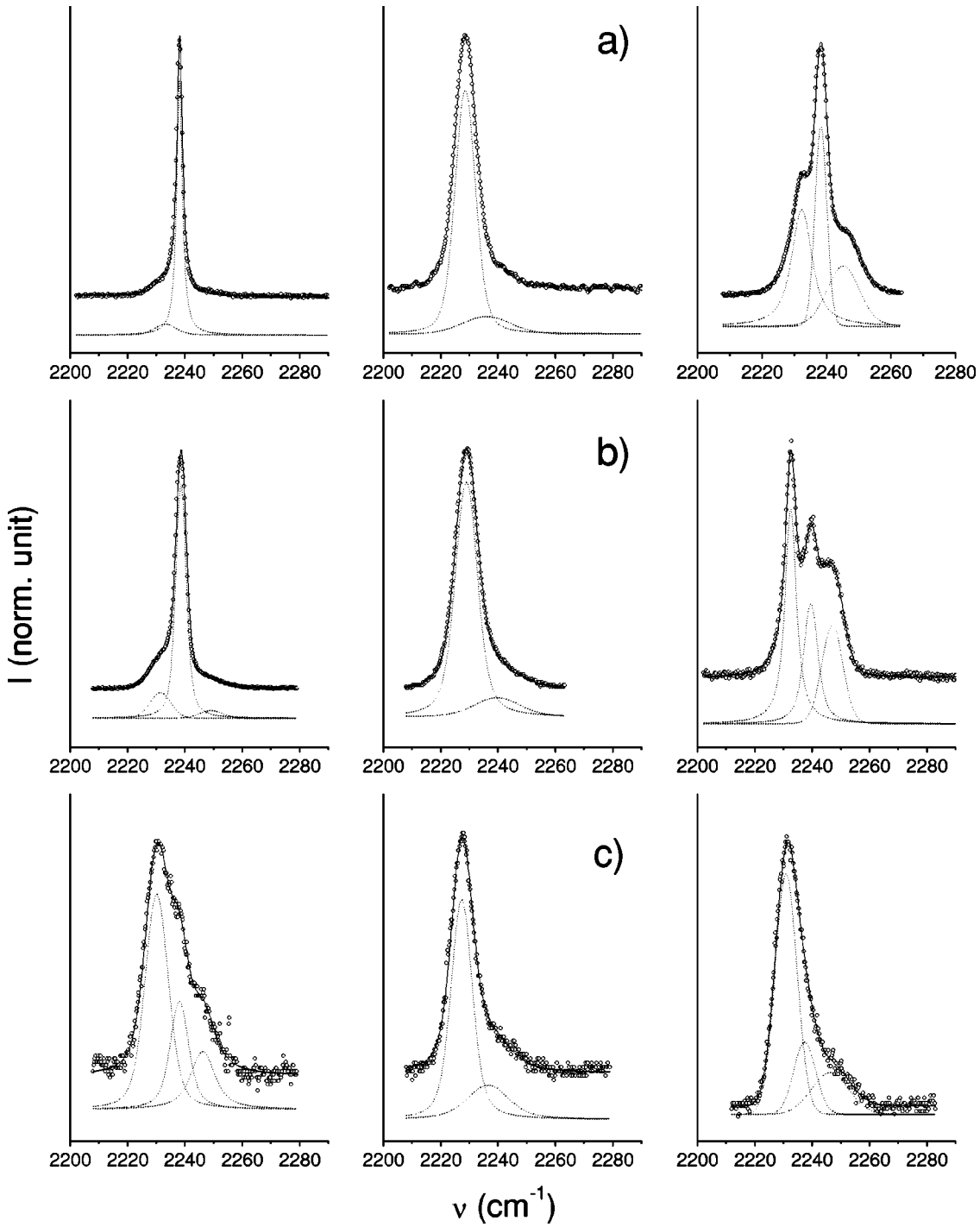

FIG. 7. Typical fits of the Raman spectra for confined 8CB in samples (a) XA20, (b) XA17, (c) XA10. Left: at 135 K after slow cooling from the isotropic phase. Center: at 320 K. Right: at 135 K after a thermal quench from the isotropic phase.

sample to another. This suggests the formation and coexistence of a limited number of phases, whose respective volumic fractions vary with confinement.

(ii) The intensity of the peak characteristic of the bulk decreases when confinement becomes more severe, i.e., when the pore size decreases and/or specific area increases. At low temperatures, this is assigned to the formation of metastable solid phases. This behavior is accentuated after a thermal quench. At high temperatures, we propose that the new component corresponds to the signature of molecules interacting with the surface, this will be discussed extensively below.

(iii) The more severe the confinement, the more important the contribution of the peak around 2230 cm^{-1} in the low temperature spectra. For a strong confinement, this peak looks very much like that measured in the liquid (crystal) phase.

(iv) The width of the peaks measured at low temperatures continuously increases with confinement, indicating smaller crystal sizes. For sample XA17 after a thermal quench, the

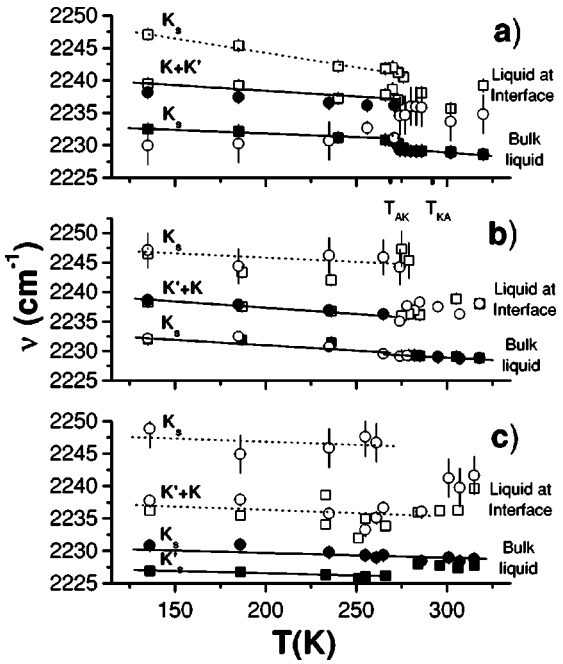

FIG. 8. Temperature dependence of the CN stretching frequency for confined 8CB in samples (a) XA20, (b) XA17, (c) XA10. Circles correspond to slow cooling from the isotropic phase. Squares correspond to slow heating after thermal quench at 100 K. Full symbols (and solid lines as guides for the eyes) correspond to the peak with the largest Raman intensity; open symbols (and dotted lines as guides for the eyes) correspond to secondary peaks. K refer to the stable crystalline phase. K', K_s, and K_s' refer to metastable solid phases (see text). T_{AK} and T_{KA} indicate the temperatures of the smectic-A–crystal and crystal–smectic-A phase transitions in the bulk.

broadening of the lowest frequency component due to smaller pore size is compensed by a narrowing due to a larger volume fraction of metastable phase.

(v) For all spectra at low temperatures, the changes in intensity and width of the highest frequency component seem to be systematically correlated with those of the lowest frequency peak, which suggests that both peaks may be assigned to the same metastable phase.

In Figure 8, we plot the temperature dependence of the frequency for each component: two at high temperatures and three at low temperatures. At high temperatures, no metastable phase is expected. Moreover, we remind that isotropic, nematic-, and smectic-A phases display approximately the same CN stretch frequency. Therefore, we propose to assign the highest frequency component to molecules in interaction with the solid surface. This suggests that the CN bond is in the vicinity of the surface and that its vibration is perturbated by some interactions with the interface. We rule out the formation of hydrogen bonds, since a strong down-shift of the frequency would be expected in this case. Within this assumption, one expects the intensity of this component to be proportional to the volume fraction of molecules in contact with the interface, $\phi_{interface}$. $\phi_{interface}$ is equal to the ratio of the specific area of the porous matrix to the surface developed by the molecules lying on a plane, which is equal to

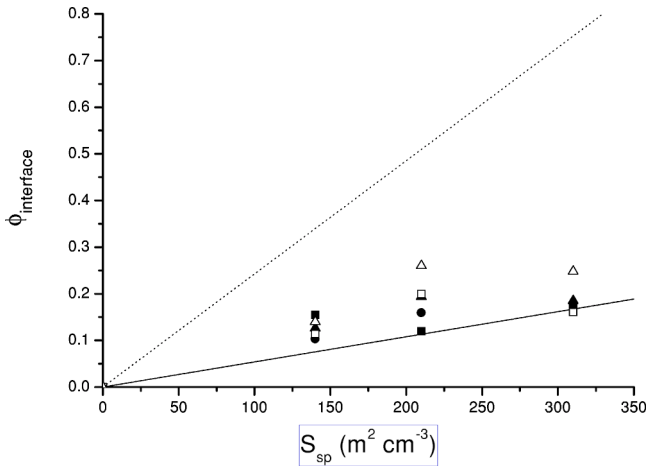

FIG. 9. Raman intensity of the highest frequency component (normalized to the intensity of the CN bunch) in the liquid phases vs interface area per unit of porous volume for the three porous matrices. Circles correspond to spectra measured at 320 K, squares at 310 K, triangles at 300 K. Solid symbols correspond to slow cooling from the isotropic phase. Open symbols correspond to slow heating after thermal quench. Solid and dotted lines correspond to trends for planar and homeotropic anchorings, respectively.

the density of molecules times the surface developed by one molecule lying on a plane. One can estimate $\phi_{interface}$ in the two extreme cases of planar and homeotropic anchorings, i.e., molecules lying preferentially parallel or perpendicular to the surface. Note that this is not straightforward to predict the nature of anchoring on the surface of porous silica matrices. Studies performed on a flat and clean silica report on planar anchoring, but the roughness of the surface and its geometry may influence the molecular orientation. In Fig. 9, we plot the intensity of the CN component assigned to molecules in interaction with the interface (normalized with respect to the total intensity of the CN bunch) as a function of the interface area per unit of porous volume S_V, which is expressed as $S_V = S_{sp}\rho/\phi_{pore}$ where S_{sp} is the specific area, ρ is the apparent mass density of the porous matrix, and ϕ_{pore} is the porosity (Table I). The solid line corresponds to the behavior expected for planar anchoring (assuming a surface of 10 nm^2 per molecule), and the dotted line to the behavior expected for homeotropic anchoring with the CN group oriented towards the surface (assuming a surface of 2 nm^2 per molecule). Note that homeotropic anchoring with the aliphatic chain oriented towards the surface is unlikely if the surface is completely covered by OH groups, as expected in the case of xeroaerogels. The rather large dispersion of the points does not allow us to conclude definitely. However, the data are in agreement with a linear dependence, which supports our assignment of the high-frequency CN component to molecules in interaction with the solid surface. Moreover, the hypothesis of pure planar anchoring provides a rather good fit of the data. Further experiments are, however, required to precise the nature and geometry of surface interactions. A quasielastic neutron scattering study of the rotational dynamics of anchored molecules, which is expected to be different for planar and homeotropic anchorings, is in progress to confirm this result.

Like in the bulk, no signature of *IN* or *AN* transition can be observed in confinement from the temperature dependence of the CN stretch. However, from the temperature dependence of the depolarization ratio (Fig. 5), several features can be observed: (i) the two plateaus characteristic of isotropic and nematic phases are still observed for samples XA20 and XA17 ; (ii) the transition is much less abrupt than in the bulk. The more severe the confinement the broader the range of temperatures between the two plateaus; (iii) the depolarization ratio in the isotropic phase are the same for bulk, samples XA20 and XA17. By contrast, ρ is slightly but significantly larger in the nematic phase for weak confinements with respect to the bulk. Finally, for sample XA10, the two plateaus can hardly be identified. This is tempting to assign these results to a change of orientational order in confined nematic phases. Such a change was also recently detected from ^{13}C NMR measurements [29]. Calculations are in progress to interpret quantitatively these changes of depolarization ratio.

At low temperatures, the splitting of the CN stretch into three components is attributed to the formation of metastable solid phases characterized by a molecular packing different than that of the stable crystalline phase. The temperature dependences of the peak frequencies are close from one sample to another. This states that there are at least two different metastable phases, each characterized by one or two components in the CN spectrum. No detail on the structure of these phases can be obtained from the Raman spectra. However, note that the temperature dependence of the low frequency peak directly extends to that of the liquid phase for samples XA10 and XA17 (Fig. 8). Therefore, this is tempting to assign this peak to the signature of a frozen-in, smecticlike phase. In the following section, we discuss the structure of the metastable solid phase(s) in the light of neutron diffraction results of the same samples.

C. Neutron diffraction signatures of the low-temperature phases

A detailed diffraction study of the structure of metastable solid phases of 8CB confined in different porous matrices will be reported elsewhere [21]. Figure 10 presents a selection of results, i.e., the neutron diffraction patterns measured at low temperature for each sample, both after slow cooling and after thermal quenching, as well as in the smectic-*A* phase. For all samples, the smectic-*A* phase is featured by a single peak at $Q \simeq 0.2$ Å^{-1}. In the bulk, the stable *K* phase is dominated by a peak at about 0.48 Å^{-1} and displays a set of five other peaks below 1.5 Å^{-1} (at 0.96, 1.15, 1.26, 1.35, and 1.42 Å^{-1}) [Fig. 10(a), left]. The results obtained upon quenching were not reproducible. As already underlined in the Raman section, this is due to the cooling speed during thermal quench which is not well controlled in our experiment and may be insufficiently large to form the metastable phase. We actually observed two kinds of patterns upon thermal quenching. One presented in the left part of Fig. 10(a), i.e., the signature of the *K* phase and the other presented in the right part of Fig. 10(a), which displays not only the series of peaks characteristic of the *K* phase but also an additional intense peak at about 0.25 Å^{-1} and other weaker peaks at about 0.64, 1.29, 1.45, and 1.53 Å^{-1}. The same series of peaks was observed in confinement for sample XA17 after slow cooling and thermal quenching [Fig. 10(c)]. An interesting result is that on these three diffractograms, the relative intensities of the four peaks at large angles are invariant, but the intensity of the peak at 0.25 Å^{-1} varies with respect to the other four peaks from a pattern to another. Therefore, we assign the series of four diffraction peaks between 0.5 and 1.6 Å^{-1} to the signature of a metastable crystalline phase, which we label K', and the peak at 0.25 Å^{-1} to another metastable solid phase. This assignment is confirmed by one of the patterns measured on sample XA20 after thermal quench and presented in Fig. 10(b). The peak at 0.25 Å^{-1} is observed to coexist with the signature of the stable *K* phase without any signature of the metastable K' phase. Note that in a recent study, Clark *et al.* reported that three peaks at 0.25, 1.28, and 1.43 Å^{-1} were measured at low temperature in bulk 8CB and were assigned to the stable crystalline phase, while two others at 0.48 and 1.15 Å^{-1} were measured at low temperature for 8CB confined in silica aerogels (of rather large pore size) and were assigned to a metastable solid crystalline phase [6]. Note also that neither of these two patterns can be indexed using the space group and lattice parameters determined recently by Kuribayashi *et al.* on 8CB monocrystals [30]. In our opinion, these contradictory results point out that two or three crystalline forms of 8CB display relatively close stabilities and that a small amount of impurities or, in a larger extent, the contact with a surface can provide nucleation conditions that favors the formation of one of these structures. Our results unambiguously state (i) that two solid crystalline phases exist and are characterized by peaks at 0.96, 1.15, 1.26, 1.35, and 1.42 Å^{-1} and at 0.64, 1.29, 1.45, and 1.53 Å^{-1}, respectively; (ii) that the peak at 0.25 Å^{-1} must be assigned to another metastable phase. Since this new metastable phase is characterized by a single diffraction peak, this is tempting to assign it to a frozen-in, smecticlike, one-dimensional crystalline order, which we labeled K_s. The cell parameter in K_s is 20% smaller than that in the smectic-*A* phase (about 2.5 nm against 3.1 nm for the smectic-*A* phase) and is likely to correspond to a packing of antiparallel dimers, such as in the smectic-*A* phase, but with a larger overlapping of the molecules. Finally, for XA10 sample, the pattern measured at low temperatures after slow cooling is dominated by the signature of phase K_s. Weak and ill-defined peaks characteristic of phase K' are observed at large angles. The most interesting feature is a single new peak at small angles (about 0.17 Å^{-1}), which is also observed with a much larger intensity after thermal quenching [Fig. 10(d)]. We assign this peak to the signature of a third metastable phase. This new phase is also likely to present a smecticlike order, such as phase K_s, but with a larger cell parameter of about 3.8 nm. We label it K_s'. Note that 3.8 nm is slightly smaller than twice the length of the molecules and therefore, one possible molecular organization for phase K_s' is a smectic packing of couples of molecules with an overlapping of the CN groups. Such a packing is observed in the crystalline structure pro-

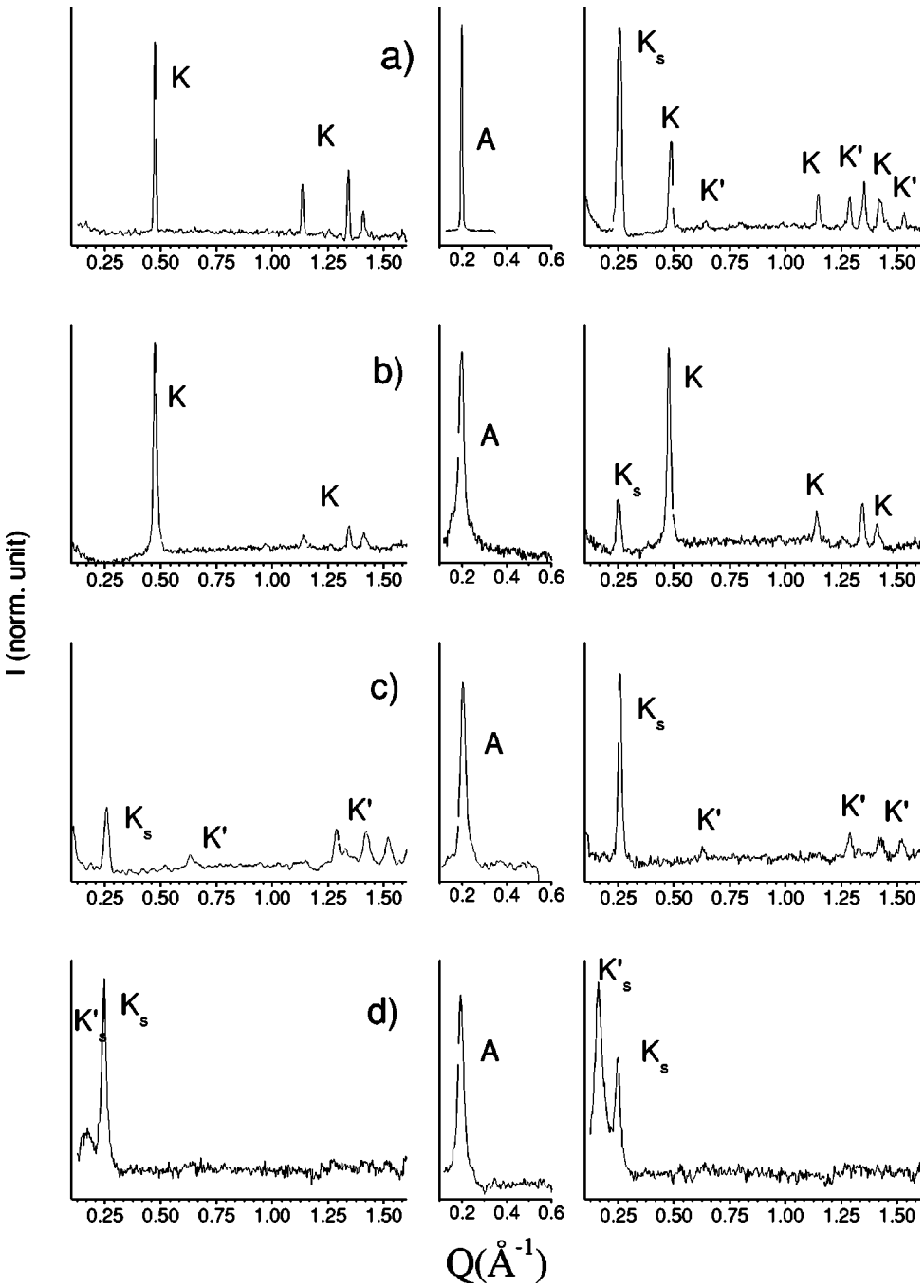

FIG. 10. Neutron diffraction patterns for 8CB at various temperatures in the bulk (a), confined in samples (b) XA20, (c) XA17, (d) XA10. Left: at 200 K after slow cooling from the isotropic phase. Center: In the smectic-*A* phase. Right: at 200 K after thermal quenching from the isotropic phase.

posed in Ref. [30] and requires only translational slippage of the molecules involved in dimers in the smectic-*A* phase.

IV. DISCUSSION

The diffraction results correlate well with the Raman ones. As far as the bulk 8CB is concerned, a slow cooling from the isotropic phase leads to a single stable crystalline phase *K*, featured by a single peak in the Raman spectrum. The behavior of the bulk 8CB after thermal quenching seems to depend on the cooling speed. With our simple setup, which consists in a thermal quench within a cooled cryostat at 100 K, two different results can be obtained :

(i) For a soft quench, the *K* phase is formed at low temperatures, its diffraction and Raman signatures are the same as that for slow cooling.

(ii) For a hard quench, the *K* phase coexists with two other phases: a metastable crystalline phase K' and a frozen-in smecticlike phase K_s. The two additional components observed in the Raman spectrum (Figs. 2 and 3) must be assigned to one (or both) of these two phases. Unfortunately, we never observed the formation of phase K' (or K_s)

alone. However, phase K_s is clearly dominating the diffraction pattern of 8CB confined in sample XA10 slowly cooled at low temperatures and, in a smaller extent, the pattern of 8CB confined in sample XA17 after thermal quenching. In both cases, the Raman counterpart is dominated by the low-frequency peak, but the two other peaks are also observed. Therefore, we state that the intrinsic spectrum of phase K_s displays an intense peak at about 2230 cm^{-1} which is the extension at low temperatures of the signature of the liquid (crystal) phases. This dominating peak is systematically associated with a weaker peak (roughly one-third of the intensity of the dominant peak) at about 2248 cm^{-1}. The intermediate peak, at about 2238 cm^{-1}, may also be a part of the intrinsic signature of phase K_s, since it is observed in the low-temperature Raman spectra of sample XA10. However, its observation in the spectra of sample XA10 is more likely to mean that a small amount of crystalline phase (K or K') is formed, but that crystalline domains are too small to give well-resolved structures in the neutron diffraction pattern. It looks like the Raman signature of phase K_s' is close to that of phase K_s. Indeed, the spectrum of 8CB in sample XA10 after thermal quench is close to that after slow cooling, while the neutron data indicate that phase K_s' is the dominant phase. However, one observes a small but significant down-shift of the lowest frequency peak for quenched sample XA10 [Fig. 9(c)] with respect to slowly cooled sample XA10, and it is therefore tempting to assign this down-shift to the intrinsic signature of phase K_s'. This down-shift indicates a slightly weaker CN stretching force constant with respect to phase K_s which is well correlated with the larger cell parameter for K_s' as compared to K_s. Finally, the metastable crystalline phase K' is observed in sample XA17 and in the bulk after quench. In both cases, it coexists with phase K_s. In addition to the intrinsic signature of K_s, the Raman spectrum displays an intense peak at 2238 cm^{-1}, which we therefore assign to the intrinsic signature of phase K'. Further diffraction data will be necessary to resolve the structure of phase K'. However, the Raman results indicate that the CN oscillators couple the same way in phases K and K' which suggests similitudes in the microscopic structure in the vicinity of the CN group. From the discussion above, we can now assign each peak of the CN bunch at low temperatures. These assignments are recalled in Figs. 8 and 10.

We now discuss the physical origin formation of the metastable phases. It is known that rodlike molecules gain stability by a parallel (or antiparallel) association due to maximized intermolecular forces. Smectic arrangements are therefore more favorable than nematic ones. Upon quenching, the sudden increase of viscosity prevents the director of the smecticlike configurations from relaxing to their appropriate equilibrium conditions, which explains the formation of frozen-in, smecticlike structures, as proposed by Perrot *et al.* [17]. There is a peculiar analogy between the effects of thermal quenching and confinement. A ''quenched disorder'' is imposed by the disordered porous matrix because of molecular anchoring. This prevents the interfacial molecules from out of axis rotating (and from axis rotating in case of planar anchoring). By contrast, translational slippage is allowed, and leads possibly to smecticlike packing but not to crystalline packing. Since rotation about the main axis (spinning motion) is also allowed (for homeotropic anchoring at least), one can get a closer packing of adjacent biphenyl groups, leading to a smaller cell parameter with respect to the smectic-*A* phase. This may explain the formation of phase K_s. Therefore, this is probably the nature and strength of molecular anchoring which govern the formation of metastable solid phases. The specific surface developed by the matrix, rather than the pore size, appears to be an important parameter to control the properties of LC in confinement. Confinement in matrices of controlled texture is an alternative and interesting approach for the study of solid crystalline polymorphism, since it offers a wide choice of experimental configurations.

V. CONCLUSION

The structure and vibrational dynamics of stable and metastable phases of 8CB was studied by Raman spectroscopy. Confinement in disordered porous matrices offers various and controllable experimental conditions to form and investigate metastable phases. This approach is an interesting alternative to the classical route by thermal quenching. Three metastable solid phases of 8CB were identified. One (K') is a crystalline phase with a structure different than that of the stable crystalline phase *K*, but with a vibrational dynamics of the CN very close to that in phase *K*. Two frozen-in, smecticlike structures (phases K_s and K_s') were also identified. These are characterized by an intrinsic Raman spectrum very different than that of the crystalline phase, which reminds in part the spectrum of the liquid (crystal) phases. On the other hand, in the liquid (crystal) phases, all the Raman spectra in confinement display a component that can be assigned to the molecules interacting with the surface of the silica network. This component is an interesting probe to investigate the anchoring of molecules on disordered surfaces.

ACKNOWLEDGMENTS

We gratefully thank B. Deme, G. Fragneto, and I. Mirebeau for their help in ND experiments. This work was achieved in the framework of a bilateral French-Venezuelian cooperation program PCP, financial support from PCP is gratefully acknowledged. We especially thank A. Hasmy, C. Goze-Bac, M. Brunet, T. Woignier, and J. Primera for stimulating interactions.

[1] *Dynamics in Small Confining Systems V*, edited by J.M. Drake, J. Klafter, P. Levitz, R.M. Overney, and M. Urbakh, MRS Symposia Proceedings No. 651 (Materials Research Society, Pittsburgh, 2001).

[2] Proceedings of Dynamics in Confinement 2000, edited by B. Frick, R. Zorn, and H. Buttner [J. Phys. IV **10** (2000)].

[3] *Liquid Crystals in Complex Geometries*, edited by G. Crawford and S. Zumer (Taylor and Francis, London, 1996).
[4] T. Bellini, N. Clark, C. Muzny, L. Wu, C. Garland, D. Schaefer, and B. Oliver, Phys. Rev. Lett. **69**, 788 (1992).
[5] B. Zhou, G.S. Ianachionne, C.W. Garland, and T. Bellini, Phys. Rev. E **55**, 2962 (1997).
[6] N. Clark, T. Bellini, R. Malzbender, B. Thomas, A. Rappaport, C.D. Muzny, D.W. Schaefer, and L. Hubesh, Phys. Rev. Lett. **71**, 3505 (1993).
[7] H. Zeng, B. Zalar, G.S. Ianachionne, and D. Finotello, Phys. Rev. E **60**, 5607 (1999).
[8] T. Bellini, M. Buscaglia, C. Chiccoli, F. Mantegazza, P. Passini, and C. Zannoni, Phys. Rev. Lett. **85**, 1008 (2000).
[9] B.J. Bulkin, K. Brezinsky, and T. Kennelly, Mol. Cryst. Liq. Cryst. **55**, 53 (1979).
[10] K. Ogorodnik, Acta Phys. Pol. A **55**, 935 (1979).
[11] V.K. Dolganov, M. Gal, N. Kroo, L. Rosta, and J. Szabon, Liq. Cryst. **2**, 73 (1987).
[12] G. Pepy, R. Fouret, M. More, and L. Rosta, Phys. Scr. **39**, 485 (1989).
[13] A. Elouatib, C. Gors, and R. Fouret, Liq. Cryst. **9**, 539 (1991).
[14] T. Mansare, C. Gors, and M. More, J. Therm. Anal. Calorim. **51**, 823 (1998).
[15] K. Hori, M. Kurosaki, H. Wu, and K. Itoh, Acta Crystallogr., Sect. C: Cryst. Struct. Commun. **C52**, 1751 (1996).
[16] M. Jaffrain, G. Lacrampe, and G. Martin, J. Phys. (France) Lett. **45**, 1103 (1984).
[17] M. Perrot, J.M. de Zen, and W.G. Rotschild, J. Raman Spectrosc. **23**, 633 (1992).
[18] J.M. De Zen, Ph.D. thesis, Université Bordeaux I, 1992 (unpublished).
[19] W.G. Rotschild, M. Perrot, and J.M. de Zen, J. Chem. Phys. **98**, 3571 (1993).
[20] P. Dieudonné, S. Calas, C. Fehr, J. Primera, T. Woignier, P. Delord, and J. Phalippou, J. Phys. IV **10**, 73 (2000).
[21] C. Fehr, P. Dieudonné, J. Primera, T. Woignier, J. L. Sauvajol, and E. Anglaret (unpublished).
[22] G. Gray and A. Mosley, Mol. Cryst. Liq. Cryst. **75**, 71 (1976).
[23] E. Galbiati and G. Zerbi, J. Chem. Phys. **84**, 3509 (1985).
[24] K. Miyano, J. Chem. Phys. **69**, 4807 (1978).
[25] P. Gautier, M. Brunet, J. Grupp, J.L. Sauvajol, and E. Anglaret, Phys. Rev. E **62**, 7528 (2000).
[26] A. Leadbetter, J. Durrant, and M. Rygman, Mol. Cryst. Liq. Cryst. **34**, 231 (1977).
[27] D. Guillon and A. Skoulios, Mol. Cryst. Liq. Cryst. **91**, 341 (1983).
[28] S.P.S. Porto, J. Opt. Soc. Am. **56**, 1585 (1966).
[29] C. Fehr, C. Goze-Bac, E. Anglaret, and A. Hasmy (unpublished).
[30] M. Kuribayashi and K. Hori, Acta Crystallogr., Sect. C: Cryst. Struct. Commun. **C54**, 1475 (1998).